Available online at www.sciencedirect.com
SCIENCE DIRECT®
Acta Materialia 52 (2004) 1555–1563
Acta MATERIALIA
www.actamat-journals.com

Estimation of biaxial surface stress by instrumented indentation with sharp indenters

Yun-Hee Lee *, Dongil Kwon

School of Materials Science and Engineering, Seoul National University, San 56-1, Shinrim-dong, Gwanak-gu, Seoul 151-744, Republic of Korea

Received 26 August 2003; received in revised form 18 November 2003; accepted 1 December 2003

Abstract

The influence of non-equi-biaxial surface stress on the shape of indentation load versus depth curve was studied experimentally by instrumented sharp indentation tests on artificially strained samples of API X65 steel. The shifts in the indentation loads for several stressed states from that of the unstressed state had a linear relationship with average equi-biaxial stresses separated from the biaxially applied stresses. Micromechanical contact analyses for the stress-induced load shifts yielded stress values comparable to the applied in-plane stresses except for the pure shear stress state, where the effect of the applied stress on indentation plasticity is negligible. This study supports the proposition that the surface stress in an arbitrary biaxial state can be evaluated through a theoretical model combined with the ratio of two principal stress components.

Keywords: Hardness testing; Residual stress; Nondestructive testing

1. Introduction

1.1. Empirical approximation of residual stress from contact-hardness measurement

Numerous studies [1–4] have been conducted over the past 70 years to drive an empirical relationship between contact hardness and elastic residual stress. In general, Vickers [1,2] or Rockwell hardness [3] decreases under tensile surface stress and increases under compressive surface stress. Anisotropic Knoop hardness test [4] has been used to analyze the two-dimensional surface stress. The hardness responses under the residual or applied stress can be explained from the viewpoint of shear plasticity. Since the indentation pressure is compressive and acts perpendicularly to the surface, tensile surface stress increases the shear stress beneath the indenter relative to the unstressed specimen. The increase of the shear stress enhances indentation plasticity, thereby reducing the contact hardness in the tensile stress state. By the same arguments, the effects of compressive stress should be symmetrically opposite to those of the tensile stress. In addition, the surface stress of brittle ceramics has been assessed through indentation fracture tests; a minimum fracture load by Hertzian contact [5] and a size of surface crack formed by Vickers indentation [6] were used as stress-detecting parameters.

Recently an instrumented indentation technique has been developed that measures the elastic/plastic deformation responses of material as an indentation load versus depth curve [7–9]; it has aroused interest because the contact hardness can be analyzed from the deformation curve instead of by direct measurement of the size of indentation impression, as in conventional hardness tests. The indentation load versus depth curve consists of loading and unloading parts representing the elastic/plastic contact deformation and elastic recovery, respectively. The indentation loading part was sensitive to the elastic surface stress and showed a lower slope (or rightward shift) in the tensilely stressed sample than in the unstressed sample and a higher slope (or leftward shift) in the compressively stressed sample. The contact hardness analyzed from the indentation unloading part showed a stress-dependency similar to that of conventional Vickers or Rockwell hardness [1–3]. Thus the

* Corresponding author. Tel.: +82-2-880-8025; fax: +82-2-889-4380.
E-mail address: uni44@mmrl.snu.ac.kr (Y.-H. Lee).

1359-6454/$30.00 © 2003 Acta Materialia Inc. Published by Elsevier Ltd. All rights reserved.
doi:10.1016/j.actamat.2003.12.006

effect of stress on contact hardness has gained new importance as it pertains to the measurement of thin-film contact hardness using an extremely low load instrumented indentation or nanoindentation technique [10–12]. However, the alteration in the contact hardness by the elastic residual stress was less than 10% of its value in the unstressed sample [13,14]. Furthermore, the current analysis [9] of the indentation unloading curve for the contact depth and hardness is based on Sneddon's solution [15] for an elastic stress field within an unstressed homogeneous half space, so that this analysis ignores the contribution of the elastic surface stress to material deformation and thus underestimates or overestimates the contact hardness [16].

1.2. Theoretical approaches for assessing residual stress

Tsui et al. [14] studying the influence of in-plane stress on indentation plasticity by investigating both the shape of the indentation curve and the contact impressions, reported that the contact hardness was invariant regardless of the elastically applied stress; this became a significant assumption of several theoretical models and was supported by subsequent finite element analysis [17]. The FEA results showed the important role of sink-in or pile-up deformations around the contact in the stressed state in producing the stress-insensitive contact hardness. A theoretical model using a geometrically similar sharp indenter has been proposed by Suresh and Giannakopoulos [18] to characterize the equi-biaxial thin-film stress. In this model, the contribution of the preexisting elastic stress to indentation plasticity is extracted as a differential contact stress in the uniaxial state, and then the ratio of true contact area of stressed and unstressed samples indented to a prescribed depth is formulated as the terms of the elastic residual stress and contact hardness. Other researchers [19] also reported the usefulness of the contact-area ratio as a parameter indicating residual stress. The differential contact stress, however, still includes a plastic-deformation-independent hydrostatic stress component, and direct measurement of the true contact area for each stress state is troublesome procedure. Lee and Kwon [20] modified the sharp-indentation model by separating a plastic-deformation-interactive deviatoric stress component from the elastic residual stress and by describing contact recoveries during a depth-controlled stress relaxation as an integral equation. The stress predictions for the instrumented indentation results of artificially strained disks of (1 0 0) tungsten single crystal [20] and rectangular beam specimen of SS 400 steel [21] showed that the modified model can measure the residual surface stresses in the equi-biaxial and uniaxial states. Taljat and Pharr [22] have recently suggested that the instrumented indentation with a spherical indenter can reveal stress effects more clearly. Swadener et al. [23] proposed contact pressure at initial yielding as a stress indicator by analyzing the elastic and elastic/plastic deformations beneath the spherical indenter.

Since the aforementioned experiments and theoretical models, however, use symmetric indenters of spherical, conical or pyramidal configuration and treat the residual surface stress in the equi-biaxial or uniaxial state only, the magnitude of the average stress effect can be determined through the instrumented indentation technique but the direction and magnitude of a principal individual stress cannot. This obstructs wide applications of the instrumented indentation technique to complex surface stress states in actual structures. A recent study by Giannakopoulos [24] also pointed this limitation of the instrumented indentation technique. In this paper, we try to verify the influence of a non-equi-biaxial surface stress on the shift of the instrumented indentation curve. Various two-dimensional stress states below the elastic limit are simulated on rectangular beam and cross-shaped specimens by using a specially designed bending apparatus. Several indentation curves, obtained from the instrumented indentation tests on the elastically strained specimens, are superposed and their deviations from that of the unstressed sample are discussed from the effects on indentation plasticity of the average value of and ratio between two axial components of the two-dimensional applied stress.

2. Experimental details

2.1. Instrumented indentation test for unstressed reference specimen

The material chosen for this study was API X65 steel, a thermomechanical-control-processed plate containing by weight 0.08%, C; 0.019%, P; 1.45%, Mn; 0.003%, S; and 0.31%, Si. Its average grain size smaller than 15 μm assured that indentation impressions could be made over a large number of grains, thereby avoiding complications arising from elastic and plastic anisotropy when individual grains are indented. The material has the elastic modulus 210 GPa, Poisson's ratio 0.3, and yield strength 490 MPa at room temperature. The 15-mm-thick rectangular beam and cross-shaped specimens (see Fig. 1(a)) were machined from a thick plate and was heat-treated at 600 °C for 2 h to remove internal stress. No warping was detected at the specimen after the stress-relief annealing. The specimen surface was mechanically ground and polished with 0.5 μm alumina powder for the subsequent instrumented indentation tests.

The instrumented indentation tests were carried out using an AIS 3000R system made by the Frontics, Inc. whose load and depth resolutions were 0.02 N and 0.10 μm, respectively. In order to measure the true contact area A_C, implying pile-up or sink-in effect around the

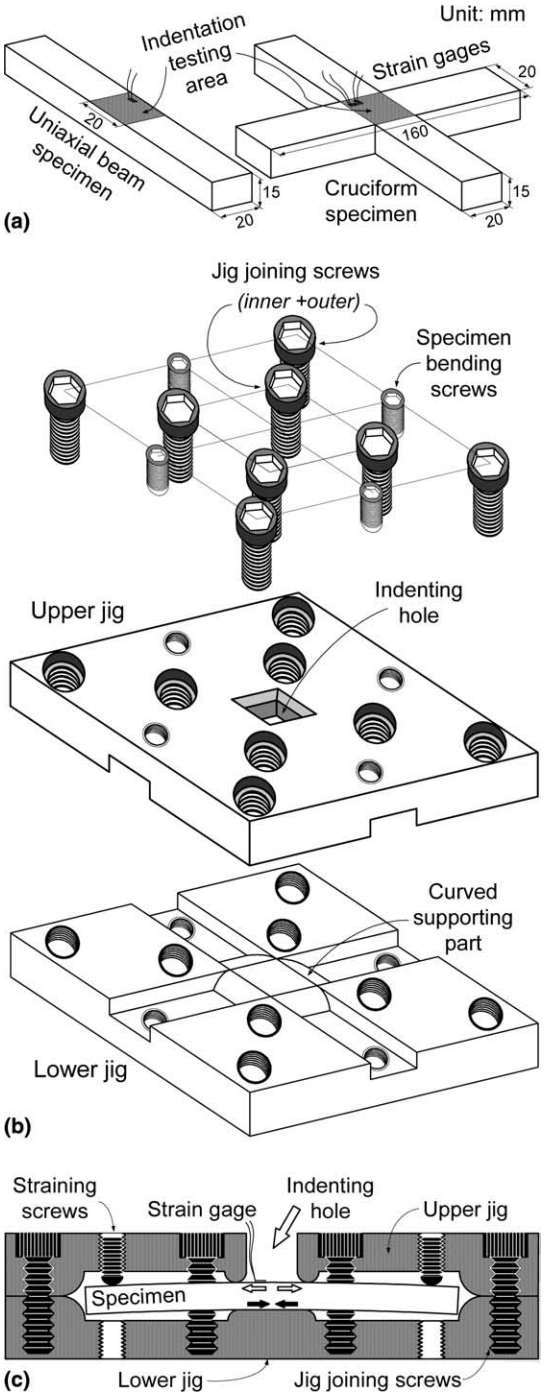

Fig. 1. Schematic diagrams of (a) rectangular beam and cruciform specimens for straining uniaxially and biaxially, respectively, (b) stress-generating apparatus; (c) cross-sectional view of the artificially bent specimen fixed in the apparatus. Subsequent indentation test can be performed on the exposed specimen surface through the indenting hole.

residual contact impression, from the conventional analysis [9] of the instrumented indentation curve, an empirical calibration for the system stiffness S_{mach} was carried out through preliminary instrumented indentation tests on the API X65 steel sample. An uncorrected stiffness S_{comb} was calculated from the gradient of the tangent to the raw indentation unloading part at the maximum indentation load and its corresponding true contact area A_C, seen in the plane of view, was directly measured through an image processing of the optical observation result. Then the two parameters were related to each other in Eq. (1), according to the conventional study on contact stiffness [9]

$$\frac{1}{S_{\text{comb}}} = \frac{1}{S_{\text{mach}}} + \frac{\sqrt{\pi}}{2E_r\sqrt{A_C}}, \tag{1}$$

where E_r is the reduced or combined modulus of the steel sample and a diamond indenter and the second term in Eq. (1), implying the true contact area A_C, is the inverse of the specimen contact stiffness. Thus, if the inverse of the machine stiffness $1/S_{\text{mach}}$, which is a discrepancy between $1/S_{\text{comb}}$ and $\sqrt{\pi}/(2E_r\sqrt{A_C})$, is empirically determined for a specimen, the raw instrumented indentation curve can be properly corrected and the true contact depth or area can be also calculated through the conventional analysis [9] of the corrected instrumented indentation curve. The empirically determined system stiffness S_{mach} for API X65 steel sample was 4.16×10^6 N/m and all instrumented indentation curves, corrected with this value, yielded the true contact depths or areas through the conventional analysis [9] of the unloading parts.

A Vickers indenter, a square-based pyramid with a 136° angle between its faces, was used in all experiments. A multi-indentation method including loading, unloading and reloading cycles at the same test location was adopted for the unstressed reference specimen to gather much contact information at different load steps at once [21]. Five indentations were made on the unstressed reference specimen with indentation load steps 98, 196, and 294 N and indentation speed 0.2 mm/min and then the instrumented indentation curves obtained were corrected using the empirically determined machine stiffness; most of the results presented here represent averages for the group. A single-indentation method with a monotonic loading–unloading cycle was also applied to the unstressed reference specimen to examine the reproducibility of the deformation curve regardless of the loading sequence.

2.2. Artificial straining and subsequent instrumented indentation test

In order to strain the rectangular beam and cruciform specimens, a stress-generating apparatus with two independent orthogonal loading axes was designed (see Fig. 1(b)). Each specimen was tightened between the upper and lower jigs using the jig-joining screws and was then biaxially loaded using the straining screws at the ends of the specimen (see Fig. 1(c)). Outer and inner jig-joining screws were located on the upper jig to

double-lock the specimen and to minimize unexpected relaxation of the elastically applied in-plane strain by the surface-normal indentation; the relaxation in the applied stain by the peak indentation load 294 N was less than 10 μ or approximate stress 2.1 MPa, negligible compared to the total applied stress. The straining screws in the upper jig created tensile strain on the exposed specimen surface whose magnitude was measured by the strain gages. By the same method, compressive strain was applied on the specimen by using the straining screws in the lower jig. The biaxially applied surface strains were converted to biaxial stresses of the two orthogonal axes using the Young's modulus and Poisson's ratio of the specimen. To keep the applied stress below the elastic limit, the difference in two orthogonal principal stress components was maintained below the specimen yield strength according to the Tresca yield criterion.

The instrumented indentation tests were also performed for the artificially stressed 20×20 mm region of the specimen center or indentation testing area in Fig. 1(a) exposed through the indenting hole, where the bending-strain is uniform along the thickness direction. A monotonic loading and unloading cycle was applied to the elastically stressed specimen with indentation load 294 N and testing speed 0.2 mm/min. Five instrumented indentation tests were repeated for each applied stress state and the raw deformation curves obtained were corrected using the machine stiffness. The applied stress was effectively constant with indentation depth because the maximum penetration achieved by the indenter, about 70 μm, was less than 0.47% of the specimen thickness. The instrumented indentation curves obtained from the biaxially stressed states were superposed on that of the unstressed reference state and the influence of the two-dimensional surface stress on the indentation deformation was analyzed.

3. Results and discussion

3.1. Measurement of contact hardness from instrumented indentation curve

The instrumented indentation curves from the multi- and single-indentation tests for the unstressed API X65 steel overlap each other perfectly in Fig. 2, ensuring that the different loading sequence has no influence on the deformation response. To analyze the corrected indentation results in Fig. 2 by Oliver–Pharr analysis [9], the unloading part was fitted to a power-law function of the indentation depth $L = k_U(h_{max} - h_f)^{m_U}$, where h_{max} and h_f are the peak indentation depth and residual indentation depth of each load step, respectively. k_U and m_U are experimentally determined fitting constants. The true contact depth h_C under the peak indentation load L_{max} is expressed as

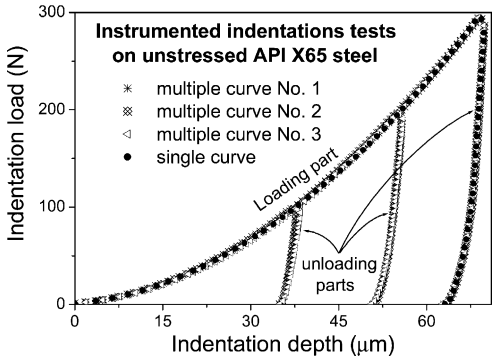

Fig. 2. Reproducible single- and multi-indentation curves of unstressed API X65 steel.

$$h_C = h_{max} - \omega \frac{L_{max}}{S_{spec}}, \tag{2}$$

where ω is the indenter geometry constant (for the Vickers pyramidal indenter, the value 0.72 for a conical indenter was used) and S_{spec} is the experimentally measured contact stiffness of the specimen, i.e., the value corresponds to the gradient of the tangent to the corrected unloading curve at h_{max}. h_C in Table 1 was converted to the true contact area A_C, i.e., the indentation area seen in the plane of view, using the geometrical relation $A_C = 24.5h_C^2$ of the Vickers indenter. Details on the true contact data obtained at each unloading part are summarized in Table 1. The contact hardness H, calculated from L_{max}/A_C, decreases slightly with increasing the indentation load L (see Fig. 3). This behavior, like the indentation size effect [25], was expressed as a power-law function of the reciprocal of indentation load $H = k_I L^{-m_I}$, where k_I and m_I are empirical fitting constants. Thus the load-dependency of the true contact area was formulated as $A_C = L^{m_I+1}/k_I$ and was also used for the artificially stressed state because, according to previous results [14,17], the true contact area or hardness is independent of the elastic residual stress state.

3.2. Influence of biaxial applied stress on shifting response of indentation curve

The six stress states, applied to the rectangular beam and cross-shaped specimens using the stress-generating apparatus in Fig. 1(b), were divided into four categories: uniaxial ($\sigma_x^{app} \neq 0$, $\sigma_y^{app} = 0$: #3 and #5), equi-biaxial ($\sigma_x^{app} = \sigma_y^{app} \neq 0$: #1 and #6), biaxial ($\sigma_x^{app} \neq \sigma_y^{app} \neq 0$:

Table 1
True contact data analyzed from the corrected unloading curves for unstressed API X65 steel

Peak load, L_{max} (N)	Peak depth, h_{max} (μm)	Residual depth, h_f (μm)	True contact depth, h_C (μm)
98	38.0 ± 0.1	35.2 ± 0.1	36.5 ± 0.1
196	55.6 ± 0.2	51.0 ± 0.2	53.6 ± 0.1
294	69.7 ± 0.1	63.3 ± 0.1	67.2 ± 0.1

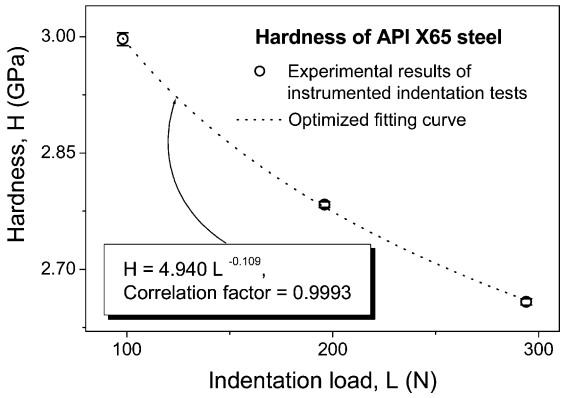

Fig. 3. Contact hardness as a function of indentation load for the unstressed specimen.

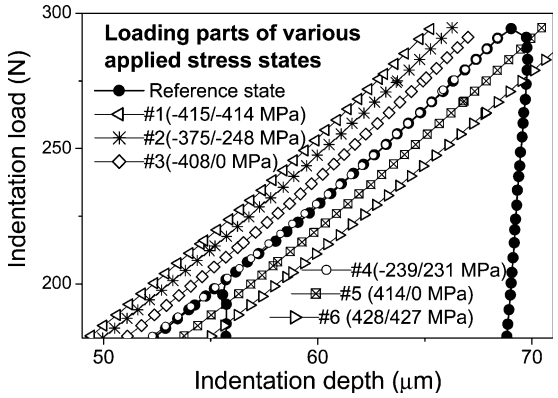

Fig. 4. Load–depth results for Vickers indentation of API X65 steel specimen in various biaxial stress states. Note that the indentation curve for the pure shear stress state (#4; open circles) overlaps and takes place no effect of the applied stress on the unstressed reference curve (solid circles).

#2), and pure shear ($\sigma_x^{app} = -\sigma_y^{app} \neq 0$: #4) states (see Table 2). We denoted one major stress component of the biaxial applied stress as σ_x^{app} and the other as a minor stress component σ_y^{app}; σ_y^{app} can be expressed as $\kappa\sigma_x^{app}$ using a stress ratio κ or $\sigma_y^{app}/\sigma_x^{app}$, where κ ranges from -1.0 in the pure shear stress through zero in the uniaxial stress to 1.0 in the equi-biaxial stress states.

The relative location of the representative indentation curve corresponding to each biaxially stressed sample is compared to that of the unstressed reference sample in Fig. 4. The indentation load of the compressively or tensilely stressed sample was higher or lower than that of the unstressed sample at a given indentation depth, as expected. From the viewpoint of shear plasticity, the increase (or decrease) of the maximum shear stress under the tensile (or compressive) stress state enhances (or constrains) indentation plasticity, thus producing a lower (or higher) indentation load than in the unstressed state for the same indentation depth. To scrutinize the stress effects on indentation plasticity quantitatively, the loading curves of the biaxially stressed and unstressed reference samples were fitted as $L = k_L h^{m_L}$ (see Table 2) rather than a quadratic function $L = k_{LV} h^2$ dependent on the Vickers pyramidal geometry, since better fitting was achieved with the power-law function. k_L, m_L, and k_{LV} are fitting constants. Among the reasons that the power-law fitting is more suitable are [26]: the work-hardened layers induced by mechanical polishing on the surface of steel samples influence the deformation response, there is friction between the indenter and sample surface, and the material under test is not ideally homogeneous. Shifts in the indentation loads of the equi-biaxially stressed states (#1 and #6) from that of the unstressed curve (reference state) were approximately twice those of the uniaxially stressed states (#3 and #5), while the indentation load of the pure shear stress state (#4) showed no shift from that of the unstressed reference state at a prescribed depth, as might be expected in the previous numerical approach [24].

The negligible stress effect on the resulting indentation curve of the pure shear state can be qualitatively understood from the relative location of and interaction between the stress-probing indenter and artificially stressed specimen surface. Since the Vickers indenter with fourfold symmetry has contacts nearly identical to the two stress-applying directions, the average effect of the in-plane pure shear stress is acquired along the unique indenter column; the increase in the indentation load by the compressive stress along one axis negates the symmetrically opposite load decrease by the tensile stress component along the orthogonal axis, thereby displaying no effect of the pure shear stress. The amount of the indentation load shift is explained with the average stress part extracted from the two-dimensional

Table 2
Analysis of indentation loading curves for the unstressed reference and artificially stressed states

Stress state	σ_x^{app} component (MPa)	σ_y^{app} component (MPa)	Stress ratio, κ ($= \sigma_y^{app}/\sigma_x^{app}$)	k_L (N/μm^{m_L})	m_L
Reference	0	0	(unstressed)	0.156 ± 0.007	1.781 ± 0.011
#1	−415	−414	1.0 (equi-biaxial)	0.162 ± 0.012	1.797 ± 0.018
#2	−375	−248	0.66 (biaxial)	0.172 ± 0.013	1.776 ± 0.016
#3	−408	0	0 (uniaxial)	0.191 ± 0.003	1.743 ± 0.006
#4	−239	231	−0.97 (pure shear)	0.159 ± 0.003	1.777 ± 0.005
#5	414	0	0 (uniaxial)	0.132 ± 0.003	1.811 ± 0.005
#6	428	427	1.0 (equi-biaxial)	0.117 ± 0.004	1.830 ± 0.006

applied stress. The biaxial applied stress σ^{app} is decomposed an average or equi-biaxial stress σ^{app}_{avg} and a pure shear stress σ^{app}_{she} parts as shown in

$$\underbrace{\begin{pmatrix}\sigma_x^{app} & 0 & 0\\ 0 & \sigma_y^{app} & 0\\ 0 & 0 & 0\end{pmatrix}}_{\text{Biaxial surface stress }(\sigma^{app})} = \underbrace{\begin{pmatrix}(1+\kappa)\sigma_x^{app}/2 & 0 & 0\\ 0 & (1+\kappa)\sigma_x^{app}/2 & 0\\ 0 & 0 & 0\end{pmatrix}}_{\text{Average or equi-biaxial stress part }(\sigma^{app}_{avg})} + \underbrace{\begin{pmatrix}(1-\kappa)\sigma_x^{app}/2 & 0 & 0\\ 0 & -(1-\kappa)\sigma_x^{app}/2 & 0\\ 0 & 0 & 0\end{pmatrix}}_{\text{Pure shear stress part }(\sigma^{app}_{she})}. \quad (3)$$

Only the average stress part shifts the indentation load and affects the indentation plasticity because the effect of the pure shear stress part does not appear on the unstressed indentation curve, as observed in Fig. 4. Similar to the load shifting behavior in an artificially stressed state, the magnitudes of average stresses of the equi-biaxially stressed states (#1 and #6) were approximately twice those of the uniaxially stressed states (#3 and #5), while that of the pure shear stress state (#4) was negligible. Thus it is confirmed that the degree of shift in the indentation load by the influence of the biaxial applied stress has a linear relationship with the average stress extracted from the biaxially applied stress (see Fig. 5). In addition, quantitative analyses were tried to predict the average stress from the stress-induced load shift.

3.3. Quantitative analysis of load shift under artificially stressed state

The theoretical indentation model of Suresh and Giannakopoulos [18] was applied to analyze the load shifts in Fig. 4. The model treated an equi-biaxial tensile stress as equivalent to a plastic-deformation-independent tensile hydrostatic stress σ^{H} plus a differential contact stress σ_z^{dif} in a negative sign along the indentation axis. A product of the differential contact stress and the contact area is the increase in the indentation load $L_0 - L_T$ brought about by relaxing the preexisting tensile surface stress (L_0 and L_T are the indentation loads, respectively, of the unstressed and tensilely stressed states indented to a prescribed indentation depth). The loads were converted to the true contact areas A_C^0 and A_C^T of the unstressed and tensilely stressed states at the same depth using the Kick's law depicting the indentation loading curve $L = k_{LV}h^2$ and the geometry of the Vickers indenter $A_C = 24.5(\alpha h)^2$, where α is a ratio of h_C/h representing the sink-in or pile-up behavior around the contact. Finally, the ratio of the true contact area A_C^T/A_C^0 was related to the average residual stress σ^{ind}_{S-G} [18]:

$$\frac{A_C^T}{A_C^0} = \left(1 + \frac{\sigma^{ind}_{S-G}}{H}\right)^{-1}. \quad (4)$$

The true contact area A_C^T in the tensilely stressed sample is determined using the load-dependency of the true contact area $A_C = L^{m_1+1}/k_I$ for the unstressed reference sample because a one-to-one relationship exists between the indentation load and the true contact area regardless of the applied stress state [14,17]. The average stresses σ^{ind}_{S-G} predicted by the Suresh and Giannakopoulos model [18] are compared to the applied average stresses σ^{app}_{avg} in Fig. 6. The predicted values (open circles) showed a linear proportional behavior but deviated from a one-to-one matching relation (plotted as a dotted line in Fig. 6) with the applied average stresses. To adjust the predicted average stresses σ^{ind}_{S-G} to the applied average stresses σ^{app}_{avg}, a multiplication by a constant near 1.4 was necessary. The reason for the discrepancy in the stress prediction was found in an improper definition of the

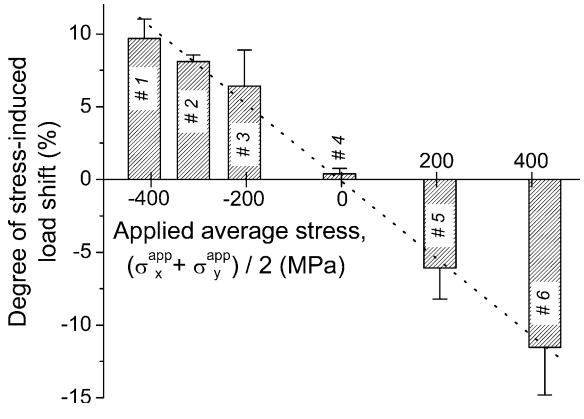

Fig. 5. Shift in indentation load as a function of applied average stress.

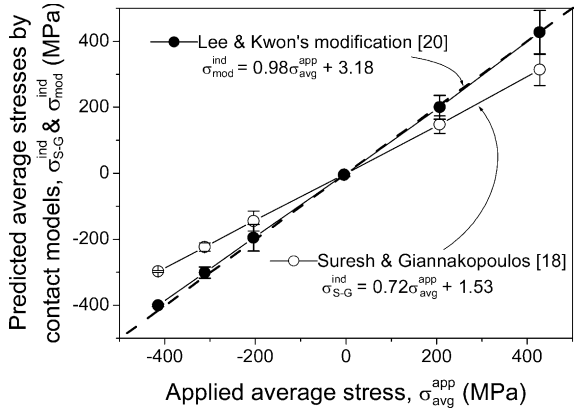

Fig. 6. Comparison of mean stresses determined from Lee and Kwon's modified model [20] with those predicted from Suresh and Giannakopoulos' initial model [18]. Note that the dotted line displays an exact match of the predicted average stress and the applied average stress.

differential contact stress σ_z^{dif} $(=-\sigma_{\mathrm{avg}}^{\mathrm{app}})$. The whole differential contact stress in the uniaxial state was assumed to influence the plastic deformation beneath the sharp indenter in the Suresh and Giannakopoulos model [18], but a plastic-deformation-independent hydrostatic stress component $\sigma_z^{\mathrm{dif}}/3$ could be still extracted from σ_z^{dif}.

Thus Lee and Kwon [20] modified the previous model [18] by decomposing the equi-biaxial tensile stress $\sigma_{\mathrm{avg}}^{\mathrm{app}}$ into a hydrostatic stress σ^{H} plus a plastic-deformation-sensitive shear deviatoric stress σ^{D}. A deviatoric stress component σ_z^{D} $(=-2\sigma_{\mathrm{avg}}^{\mathrm{app}}/3)$ parallel to the indentation axis plays a role similar to the differential contact stress in the Suresh and Giannakopoulos model [18]. A product of σ_z^{D} and its interacting area $A_{\mathrm{C}}^{\mathrm{T}}$ is equivalent to the applied stress-induced load shift $L_0 - L_{\mathrm{T}}$. If the indenter has a perfect geometry of the Vickers pyramid, the modified equation of the average stress in [20] will be simplified to Eq. (5). The self-similarity of the Vickers geometry used was experimentally identified; a line defect less than 1 μm long was found at the indenter apex from a direct indenter observation through an atomic force microscope.

$$\sigma_{\mathrm{mod}}^{\mathrm{ind}} = \frac{3(L_0 - L_{\mathrm{T}})}{2A_{\mathrm{C}}^{\mathrm{T}}}. \tag{5}$$

The superposed indentation curves from various stress states in Fig. 4 were reanalyzed according to the Lee and Kwon's modification in Eq. (5) [20]. The newly predicted average stresses $\sigma_{\mathrm{mod}}^{\mathrm{ind}}$, which are superposed on the previous results in Fig. 6, showed good agreement with the applied average stress $\sigma_{\mathrm{avg}}^{\mathrm{app}}$ within a standard deviation of ±8.57 MPa. The Eq. (4) can be rearranged a similar formulation of Eq. (5) by substituting the indentation load into the true contact area according to the definition of the contact hardness; if we neglect the variation in the contact hardness in Fig. 3, H can be expressed as L_0/A_{C}^0 or $L_{\mathrm{T}}/A_{\mathrm{C}}^{\mathrm{T}}$. Finally, Eq. (4), rearranged as $(L_0 - L_{\mathrm{T}})/A_{\mathrm{C}}^{\mathrm{T}}$, becomes the same as Eq. (5) by multiplying by a constant 3/2, a value similar to the experimentally determined modification constant 1.4.

If the stress ratio κ is already known, individual principal stress component can be also calculated from the average stress $\sigma_{\mathrm{mod}}^{\mathrm{ind}}$ using the relationship $\sigma_{\mathrm{avg}}^{\mathrm{app}} = (1+\kappa)\sigma_x^{\mathrm{app}}/2$ between the applied average stress and the individual principal stress component. $\sigma_{\mathrm{mod},x}^{\mathrm{ind}}$ is expressed as a multiple of a stress-directionality factor $3/((1+\kappa)A_{\mathrm{C}}^{\mathrm{T}})$ and the stress-induced load shift $L_0 - L_{\mathrm{T}}$. Erroneous component stresses, however, are estimated in the pure shear stress state because $3/((1+\kappa)A_{\mathrm{C}}^{\mathrm{T}})$ and $L_0 - L_{\mathrm{T}}$ converge to infinity and zero at $\kappa = -1.0$, respectively.

3.4. Stress sensitivity of instrumented indentation testing

The sensitivity of the instrumented indentation technique in measuring the residual stress is estimated by considering arbitrary stress states. Let $\sigma_{\mathrm{mod},x}^{\mathrm{ind}}$ be a fixed stress 240 MPa, and let κ decrease from 1.0 to −1.0 by continuously changing $\sigma_{\mathrm{mod},y}^{\mathrm{ind}}$ from 240 to −240 MPa. The indentation load L_{T} corresponding to each stressed state at indentation depth 70 μm was determined through a numerical iteration method; L_0 at the depth 70 μm was determined from the fitted loading curve of the unstressed reference state in Table 2 and $A_{\mathrm{C}}^{\mathrm{T}}$ was converted to a function of the indentation load or $L_{\mathrm{T}}^{m_{\mathrm{I}}+1}/k_{\mathrm{I}}$ according to Fig. 3. Then the responses of the stress-induced load shift $L_0 - L_{\mathrm{T}}$ and the stress-directionality factor $3/((1+\kappa)A_{\mathrm{C}}^{\mathrm{T}})$ were estimated, as plotted versus the stress ratio κ in Fig. 7. Multiplication of the exponentially decaying response of the stress-directionality factor and the linearly increasing behavior in the stress-induced load shift with increasing κ makes the dominant principal stress component $\sigma_{\mathrm{mod},x}^{\mathrm{ind}}$ constant except in the case of $\kappa = -1.0$, where $3/((1+\kappa)A_{\mathrm{C}}^{\mathrm{T}})$ and $L_0 - L_{\mathrm{T}}$ are infinity and zero, respectively. If we determine an resolution of the stress-induced load shift, discriminating the effects of the residual stress against the background fluctuation in the indentation load caused by the combined effects of material inhomogeneity and testing-system resolution, a stress-measurable region by the instrumented indentation technique can be estimated. The actual resolution of $L_0 - L_{\mathrm{T}}$ at maximum indentation depth 70 μm was determined to be about 1.0 N in this study. An intersection of the horizontal line for the background load fluctuation 1.0 N and the linearly increasing $L_0 - L_{\mathrm{T}}$ line against κ in Fig. 7 yielded a lower bound κ_{lim} of the stress-measurable region. We can expect that the stress prediction via the instrumented indentation technique is reasonable in the range $\kappa_{\mathrm{lim}} < \kappa \leqslant 1.0$. It is possible to estimate the surface stress properly from the experimental indentation results within the stress range $-213.5 < \sigma_{\mathrm{mod},y}^{\mathrm{ind}} \leqslant 240$ MPa because κ_{lim} is −0.89 for the fixed $\sigma_{\mathrm{mod},x}^{\mathrm{ind}}$ of 240 MPa. The

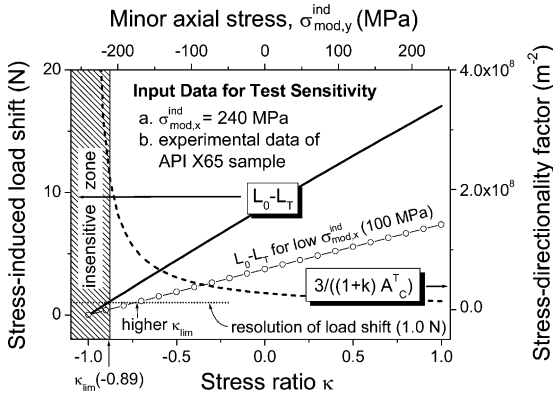

Fig. 7. A lower bound of stress-measurable region κ_{lim} for $\sigma_{\mathrm{mod},x}^{\mathrm{ind}}$ 240 MPa estimated from a comparison between the experimental resolution and response of the stress-induced load shift against the stress ratio. κ_{lim} increases with decreasing the residual surface stress due to the lower slope of the stress-induced load shift $L_0 - L_{\mathrm{T}}$ line at 100 MPa.

erroneous stress prediction in the pure shear stress state (#4; −239/231 MPa, $\kappa = -0.97$) is also to be expected.

Furthermore, the sensitivity of this indentation technique to a lower residual stress than $\sigma^{\text{ind}}_{\text{mod},x}$ of 240 MPa was also explored. The above-explained analysis was repeated for determining κ_{lim} for a given major stress component $\sigma^{\text{ind}}_{\text{mod},x} < 240$ MPa. The responses of $L_0 - L_{\text{T}}$ and $3/((1+\kappa)A^{\text{T}}_{\text{C}})$ at depth 70 μm versus κ were estimated; as the $\sigma^{\text{ind}}_{\text{mod,x}}$ decreases, the magnitude and increasing slope of $L_0 - L_{\text{T}}$ significantly decrease, while the change of $3/((1+\kappa)A^{\text{T}}_{\text{C}})$ is negligible. Thus the stress-measurable lower bound κ_{lim} increases at the low residual stress because the experimental resolution of the load shift is constant 1.0 N but the magnitude of the $L_0 - L_{\text{T}}$ line decreases as the residual stress decreases (see the $L_0 - L_{\text{T}}$ line for $\sigma^{\text{ind}}_{\text{mod},x}$ of 100 MPa in Fig. 7). κ_{lim} values estimated from various residual stress states make a solid boundary in Fig. 8 and it separates two-dimensional elastic residual stress states into stress-measurable and stress-insensitive zones by the instrumented indentation technique. A high residual stress above 200 MPa in the equi-biaxial state (or upper right zone in Fig. 8) can be easily detected by the instrumented indentation technique, while a low residual stress below 30 MPa in the pure shear stress state (or lower left region in Fig. 8) cannot. A saturation of κ_{lim} to −0.9 in the right region of Fig. 8 means that nearly all two-dimensional residual stress states except for the pure shear state ($\kappa = -1.0$) can be evaluated by the instrumented indentation test in the high residual stress level. The sensitivity of the instrumented indentation test, however, drastically decreases with the decrease of the residual surface stress (see the left region in Fig. 8); the stress-measurable range $-0.89 < \kappa \leqslant 1.0$ at $\sigma^{\text{ind}}_{\text{mod},x} = 240$ MPa, shrinks to a narrow range $0 < \kappa \leqslant 1.0$ at 26.5 MPa, and finally disappears at 13.3 MPa. This means that the residual surface stress less than 13.3 MPa cannot be measured by this instrumented indentation technique even if the stress state is equi-biaxial or $\kappa = 1.0$. Therefore, in order to assess the two-dimensional residual stress properly from the instrumented indentation results, such factors as the stress-detectable limit based on the experimental resolution of the stress-induced load shift and stress ratio of the indented location should be known.

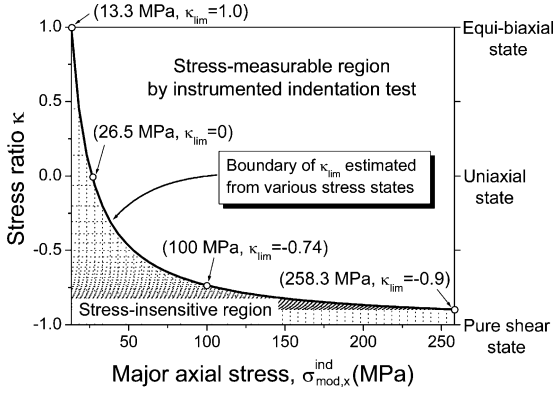

Fig. 8. κ_{lim} locus dividing stress-measurable and insensitive regions with the instrumented indentation technique. A stress state within the hatching region cannot be measured by this indentation test.

4. Conclusions

The influence of two-dimensional surface stress on the indentation load versus depth curve was studied experimentally by instrumented indentation tests on artificially strained steel samples. A shift behavior of the indentation loading curve in stressed state from that of unstressed state was qualitatively explained and its amount was analyzed into a quantitative stress value through theoretical indentation models. The major conclusions are:

1. Residual surface stresses were simulated on rectangular beam and cross-shaped samples using a stress-generating apparatus with two independent orthogonal loading axes. Two-dimensional applied stress states, expressed using a major principal stress component σ^{app}_x and a stress ratio κ or $\sigma^{\text{app}}_y/\sigma^{\text{app}}_x$, were divided into four categories: equi-biaxial ($\kappa = 1.0$), non-equi-biaxial ($-1.0 < \kappa < 0$ and $0 < \kappa < 1.0$), uniaxial ($\kappa = 0$) and pure shear ($\kappa = -1.0$) states.
2. The indentation loading curves of various applied stress states showed complex shifts from that of the unstressed reference state, while that of the pure shear stress state showed no deviance and superposed perfectly on the unstressed indentation curve. Since the two-dimensional applied stress was decomposed into equi-biaxial stress and pure shear stress parts and the latter had no influence on the indentation deformation, the stress-induced load shift could be explained only with the extracted equi-biaxial stress part.
3. The Suresh and Giannakopoulos model, applied for the analysis of the stress-induced load shifts, yielded stress predictions that are proportional to but deviates from the applied average stress. Thus the stress-induced load shift was reanalyzed with Lee and Kwon's modified model. It predicted the average stress agreeing well with the applied average stress (within a standard deviation of ±8.57 MPa). In addition, an individual principal stress component $\sigma^{\text{ind}}_{\text{mod},x}$ could be calculated from the predetermined average stress $\sigma^{\text{ind}}_{\text{mod}}$ using the following equation with information of the stress ratio κ

$$\sigma^{\text{ind}}_{\text{mod},x} = \frac{2}{(1+\kappa)}\sigma^{\text{ind}}_{\text{mod}} = \frac{3}{(1+\kappa)A^{\text{T}}_{\text{C}}} \times (L_0 - L_{\text{T}}).$$

4. The sensitivity on the residual stress of the instrumented indentation technique was scrutinized by determining the lower bound of stress-measurable region or κ_{lim}. Since κ_{lim} is very low at high stress level

approaching the yield strength, the residual stress can be easily measured by the instrumented indentation technique. But the stress-measurable range is drastically reduced with decreasing the residual stress and finally disappears at the lowest stress detectable limit. Thus the testing sensitivity and local stress ratio of specimen should be properly considered to evaluate the two-dimensional residual stress exactly by the instrumented indentation technique.

Acknowledgements

This work was supported by the Asian Office of Aerospace Research and Development/Air Force Office of Scientific Research. Parts of this work were funded by the National Research Laboratory Program of the Korean Ministry of Science and Technology.

References

[1] Sines G, Carlson R. ASTM Bull 1952;180:35.
[2] Vitovec FH. ASTM Spec Tech Publ 1985;889:175.
[3] Frenkel J, Abbate A, Scholz W. Exp Mech 1993;33:164.
[4] Oppel GU. Exp Mech 1964;4:135.
[5] Roberts SG, Lawrence CW, Bisrat Y, Warren PD, Hills DA. J Am Ceram Soc 1999;82:1809.
[6] Zeng K, Rowcliffe DJ. Acta Metall Mater 1995;43:1935.
[7] Loubet JL, Georges JM, Marchesini O, Meille G. J Tribol 1984;106:43.
[8] Doerner MF, Nix WD. J Mater Res 1986;1:601.
[9] Oliver WC, Pharr GM. J Mater Res 1992;7:1580.
[10] LaFontaine WR, Yost B, Li C-Y. J Mater Res 1990;5:776.
[11] LaFontaine WR, Paszkiet CA, Korhonen MA, Li C-Y. J Mater Res 1991;6:2084.
[12] Zagrebelny AV, Carter CB. Scripta Mater 1997;37:1869.
[13] Doerner MF, Gardner DS, Nix WD. J Mater Res 1986;1:845.
[14] Tsui TY, Oliver WC, Pharr GM. J Mater Res 1996;11:752.
[15] Sneddon IN. Int J Eng Sci 1965;3:47.
[16] Bai M, Kato K, Umehara N, Miyake Y. Thin Solid Films 2000;377–378:138.
[17] Bolshakov A, Oliver WC, Pharr GM. J Mater Res 1996;11:760.
[18] Suresh S, Giannakopoulos AE. Acta Mater 1998;46:5755.
[19] Carlsson S, Larsson PL. Acta Mater 2001;49:2179.
[20] Lee Y-H, Kwon D. Scripta Mater 2003;49:459.
[21] Lee Y-H, Ji W, Kwon D. Exp Mech 2004 [in press].
[22] Taljat B, Pharr GM. Mater Res Soc Symp Proc 2000;594:519.
[23] Swadener JG, Taljat B, Pharr GM. J Mater Res 2001;16:2091.
[24] Giannakopoulos AE. J Appl Mech 2003;70:638.
[25] Elmustafa AA, Stone DS. Acta Mater 2002;50:3641.
[26] Mencik J, Swain MV. Mater Forum 1994;18:277.